The Integrate-and-Fire Neuron Model as a Sensory Neuron Model

A Tech Brief for the Neurofuzzy Soft Computing Project

Rick Wells
Aug. 20, 2003

I. Introduction

In our previous tech brief on modeling a simple biomimetic joint, I proposed the use of the integrate-and-fire model as the model for the muscle spindle afferent sensory neurons. In the form presented previously, I used the equation for the ideal I&F neuron. In this tech brief I'd like to extend this model a bit and make it a better representative of our BAN circuit. I will also discuss some non-standard modifications to the model that make its response give a better reproduction of the biological behavior of the spindle afferent sensory neurons which produce the type Ia afferent feedback signal from the muscle spindle.

The general scheme of the I&F neuron is shown below in Figure 1. Neglecting the synaptic inputs and their synaptic weights, the model consists of only two components. The first is a leaky integrator receiving input signal V (which represents the weighted and summed input signals) and producing integrator output signal y. The LI is described by the differential equation

$$\dot{y}(t) = -\frac{1}{\tau_n} y(t) + \frac{1}{\tau_n} V(t) \qquad (1)$$

where τ_n is the time constant of the integrator. Immediately after the neuron has fired a pulse the

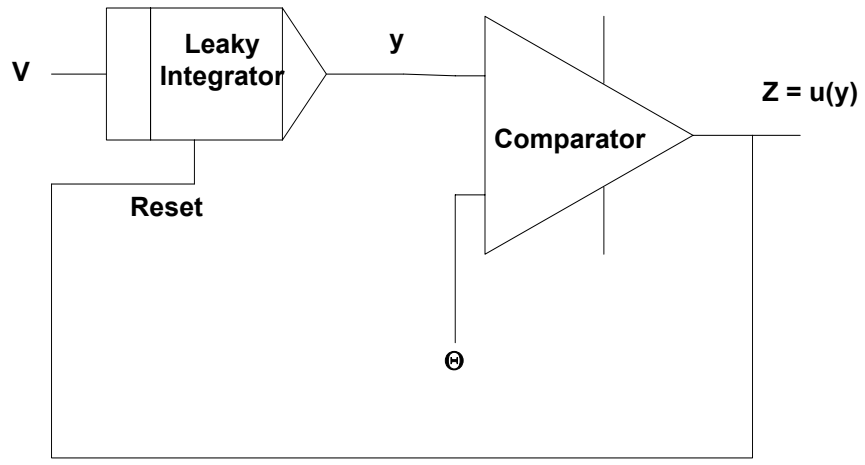

Figure 1: Integrate-and-Fire Neuron Model. The I&F neuron model consists of two components, not including the summing of the synaptic inputs. Summed input V is applied to a leaky integrator, which produces output y. When y exceeds the threshold Θ at the input to the comparator, the comparator produces an output of 1. Otherwise the comparator output is 0. The output is fed back to reset the leaky integrator, returning y = 0. The LI has unity dc gain, time constant τ_n , and reset time t_r .

initial condition of the integrator is reset to $y = 0$ and the integration action resumes. The LI output is applied to one input of a comparator; the other comparator input is a threshold Θ. The comparator output z is zero when $y < \Theta$ and is one when $y \geq \Theta$. When z goes high, the feedback from the comparator to the LI resets the integrator. We will assume that t_r is the time required to reset the integrator. In the *ideal* integrate and fire neuron $t_r = 0$. (That assumption was quietly employed in the "Joint" tech brief; for very good reasons, we will abandon this idealization in this tech brief). Because of the reset action, the LI during integration is completely described by the Laplace transform transfer function

$$H(s) = \frac{1}{s\tau_n + 1} \tag{2}.$$

We may note that this transfer function has unity dc gain (H when s is zero). In the previous tech brief, the I&F equation presented was for an LI that did not have unity dc gain, and this is going to make a slight (and unimportant) difference in the firing rate equation we will derive here.

The steady-state firing rate of the I&F neuron is defined for a step input for V. If V is a step function of amplitude V_t the response at the LI's output is

$$y(t) = V_t\left(1 - e^{-t/\tau_n}\right)u(t) \tag{3}$$

while the comparator output $z = 0$. In order to fire an action potential, y must achieve the value of the threshold Θ. Therefore, for $V_t < \Theta$ the firing rate R is equal to zero (since the neuron does not fire at all). Assuming y is capable of exceeding the threshold, the time required for y to integrate up to the threshold value is found by solving (3) under the condition $y = \Theta$, which gives the time to the firing point as

$$t_f = -\tau_n \ln\left(1 - \frac{\Theta}{V_t}\right) \tag{4}.$$

Because the neuron cannot fire again until the reset operation is completed, the interval between action potentials is $T = t_r + t_f$. This gives us a firing rate

$$R = \frac{1}{t_r + t_f} = \frac{1/\tau_n}{(t_r/\tau_n) - \ln(1 - (\Theta/V_t))} \tag{5}.$$

In the limit where $t_r << \tau_n$, this expression reduces to the ideal I&F expression given in the "Joint" tech brief (except for the absence of the time constant inside the natural logarithm; this is due to our use of a unity gain integrator in the model here).

The maximum firing rate of the neuron occurs then the logarithm term goes to zero, which happens when V_t goes to infinity. (By definition, V_t must always be non-negative for (5) to apply; when V_t goes negative, it is less than threshold and the neuron doesn't fire at all). This maximum firing rate is

$$R_{\max} = \frac{1}{t_r} \tag{6}.$$

We see here that the reset time determines the maximum firing rate of the neuron. For the ideal I&F neuron, there is no limit to how fast it can fire, and this is not a physically reasonable state of affairs. None of our artificial neuron circuits have zero reset time, nor do any biological neurons. The need to impose an upper limit on firing rate leads to some modifications we must make to our previous modeling work on spindle afferents. Specific data on biologically realistic maximum neuronal firing rates is sparse, but I have selected 400 impulses/sec (t_r = 2.5 msec) as a reasonable maximum value for the models presented here.

II. Modifications to the Primary Afferent Model

There is an additional modification we need to make for the spindle primary afferent sensory neuron (the type Ia sensor). In part II of the "Joint" tech brief I proposed the simplest model of the receptor potential in a spindle afferent sensory neuron as

$$V_t = \sum_{\forall b} V_r^{(b)} + \sum_{\forall c} V_r^{(c)} \tag{7}$$

where $V_r^{(b)}$ is the receptor potential due to a bag fiber and $V_r^{(c)}$ is the receptor potential due to a chain fiber. The experimental data we examined previously supports the hypothesis that sensory nerve endings on bag 2 and on chain fibers respond merely to the length x_s of the spindle region, which for the Hill model is given by the length of the series elastic component (SEC). For a bag 2 or a chain fiber we then have

$$V_r = a \cdot x_s$$

where a is the sensitivity of the nerve ending and is analogous to synaptic weight. Let us therefore make the hypothesis that

$$V_r^{(b2)} + \sum_{\forall c} V_r^{(c)} = a_1 \cdot \bar{x}_s \tag{8}$$

where $\bar{x}_s$ is the average of the spindle lengths of the bag 2 and chain spindles and a_1 is an overall proportionality factor. Because bag 2 and chain fibers appear to have the same (or very similar) mechanical parameters (e.g. stiffness ratio, pole frequency, and zero frequency), $\bar{x}_s$ will be primarily a function of the fusimotor excitation applied to each different intrafusal fiber[1] and, of course, the length of the muscle determined by the extrafusal muscle fibers.

The bag 1 fiber differs from the others in that the experimental evidence indicates that the nerve endings in the bag 1 spindle are primarily sensitive to the time rate of change (velocity) of the bag 1 SEC. We furthermore have the experimental observation that negative velocities (contraction) in the fiber length causes an interruption or break in the firing of the Ia afferent. This strongly suggests that negative velocities produce a hyperpolarizing response in the sensory neuron, which leads to the simplest model for receptor potential from a bag 1 nerve ending as

$$V_r^{(b1)} = a_2 \dot{x}_{b1} + a_3 x_{b1}$$

[1] Fusimotor excitation means excitation by the action potentials of gamma motoneurons.

where x_{b1} is the length of the bag 1 SEC and $\dot{x}_{b1}$ is its velocity.

However, this simple model fails to correctly reproduce the behavior of the primary afferent signal. Specifically, setting the receptor potential as proportional to $\dot{x}_{b1}$ produces unrealistically high Ia firing rates as a function of velocity with model parameters that accurately represent the zero-velocity firing characteristics. This implies that there is some sort of saturation effect that sets in for high velocities $\dot{x}_{b1}$. The cause of this effect is not known, nor has the biophysical mechanism been derived. I have been able to obtain reasonably good agreement between model behavior and the experimental data up to a muscle velocity range of 40 mm/sec by using a phenomenological model

$$V_r^{(b1)} = c \cdot \tan^{-1}\left(a_2 \dot{x}_{b1}\right) + a_3 x_{b1} \tag{9}$$

where parameter *c* is an empirically-determined constant. Employing (9) we obtain the receptor potential model for the primary spindle afferent neuron as

$$V_t = a_1 \bar{x}_s + c \cdot \tan^{-1}\left(a_2 \dot{x}_{b1}\right) + a_3 x_{b1} \tag{10}.$$

This is the expression I use in obtaining the results discussed later in the next section. Note that for small values of velocity

$$c \cdot \tan^{-1}\left(a_2 \dot{x}_{b1}\right) \approx c \cdot a_2 \dot{x}_{b1}$$

which is consistent with the Matthews-Stein transfer function characteristic we discussed in the "Joint" tech brief. (Small amplitude sinusoidal length changes in the muscle produces small velocities since the velocity of a sinusoid is proportional to the amplitude of the excitation).

III. Model Parameters and Model Results

The secondary afferent (type II) sensory neuron receives no input from bag 1 fibers. Its receptor potential therefore follows (8). I obtained model parameters for the "zero-velocity" terms by fitting the firing rates of the primary and secondary afferents to experimental data at two points on the firing rate vs. muscle extension characteristic under conditions of zero fusimotor excitation using the mechanical parameters developed in part II of the "Joint" tech brief. Let R_p and R_s denote the primary and secondary firing rates, respectively. For the secondary afferent

$$R_s = \frac{R_{s0}}{\eta_s - \ln\left(1 - \Theta_s / \bar{x}_s\right)} \tag{11}$$

where $R_{s0} \equiv 1/\tau_n$, $\eta_s \equiv t_r/\tau_n$, and $\Theta_s \equiv \Theta/a_1$. The resulting parameters were

$$R_{s0} = 22.957$$
$$\eta_s = 0.05739 \ .$$
$$\Theta_s = 0.055$$

For the primary afferent we have

$$R_p = \frac{R_{p0}}{\eta_p - \ln\left(1 - \frac{\Theta_p}{\bar{x}_s + c \cdot \tan^{-1}\left(a_2 \dot{x}_{b1}\right) + a_3 x_{b1}}\right)} \tag{12}$$

where the normalized variables are defined as they were above. I fit the "zero-velocity" terms as

$$R_{p0} = 12.82327$$
$$\eta_p = 0.032085$$
$$\Theta_p = 0.20$$
$$a_3 = 1.00$$

To obtain the velocity-dependent factors I fit the primary response to two points on the experimental dynamic index curve under conditions of zero fusimotor excitation. Recall that the dynamic index is the difference between the firing rate at the peak of a ramp stretch and the steady-state firing rate 0.5 seconds after the end of the ramp. This was illustrated in figure 16 of part II of the "Joint" tech brief. The resulting parameters are

$$c = 2.70$$
$$a_2 = 1.20$$

Note that the factor $r = c \cdot a_2 = 3.24$ is a parameter in the Matthews-Stein transfer function discussed in part II of the "Joint" tech brief. This value of r produced a quite good match to the measured transfer function curve for the primary afferent.

With these parametric values the model produces results that are in reasonable agreement with experimental data. Figure 2 shows the model firing rates as a function of muscle extension over a range from 4 mm to 14 mm. The results are for the case of no fusimotor excitation. Both curves are in reasonably good agreement with experimental data.

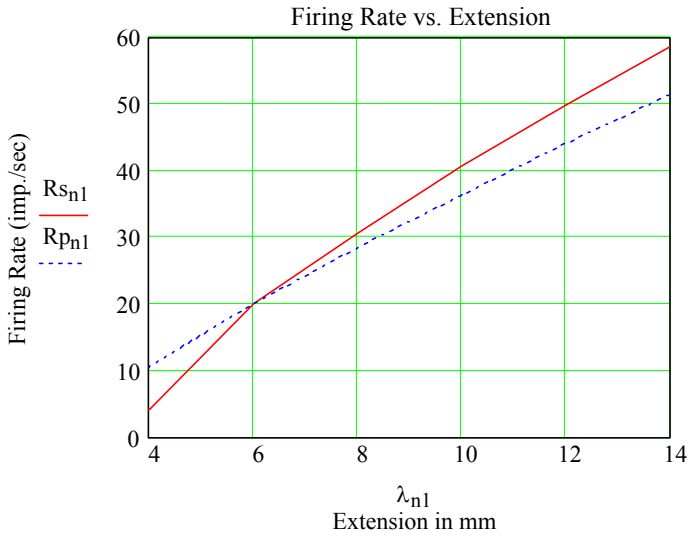

Figure 2: Firing rates vs. muscle extension with no fusimotor excitation. R_s = secondary firing rate. R_p = primary firing rate. The curves were forced to equal 20 imp/sec at λ = 6 mm.

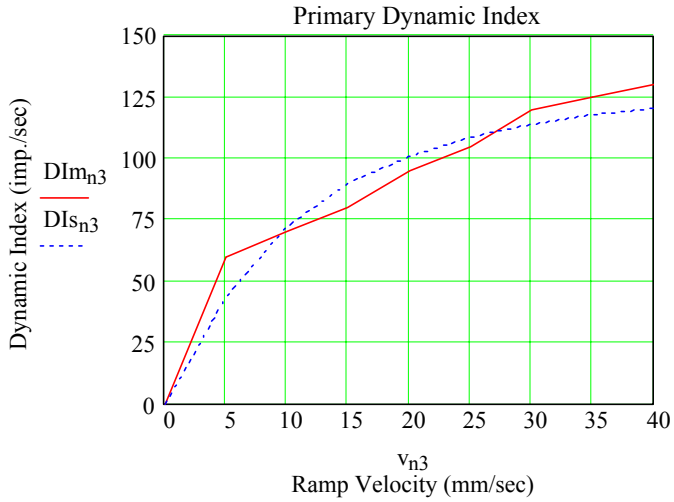

Figure 3: Measured and modeled dynamic indices for the primary afferent. The curves are for zero fusimotor excitation with an initial muscle length of λ = 5 mm and a final length of λ = 10 mm. DIm is the measured (experimental) dynamic index. DIs is the modeled dynamic index.

The dynamic index is one of the most important spindle afferent firing characteristics. Figure 3 compares the experimental vs. the modeled dynamic index for the primary afferent under conditions of zero fusimotor excitation. The agreement between measured and modeled results is quite good up to a velocity of 40 mm/sec. For velocities beyond this point the model under-predicts the dynamic index. This appears to be a consequence of the phenomenological arctangent function used in the model.

Agreement between measured and modeled results seems to be not quite as good for the secondary afferent. Figure 4 illustrates the comparison. However, the experimental data was taken from a graph of reported results, and the graph's scale did not provide very good resolution for obtaining the measured data. I therefore cannot conclude that the difference is significant.

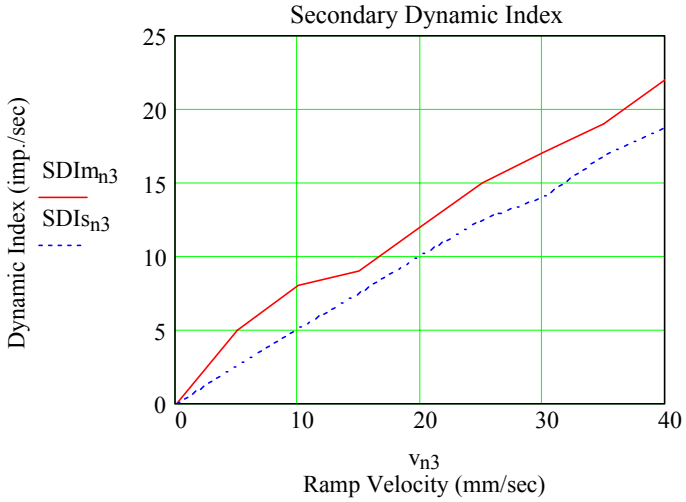

Figure 4: Measured and modeled dynamic indices for the secondary afferent. The experimental conditions are the same as for figure 3. SDIm = measured secondary dynamic index. SDIs = modeled secondary dynamic index.

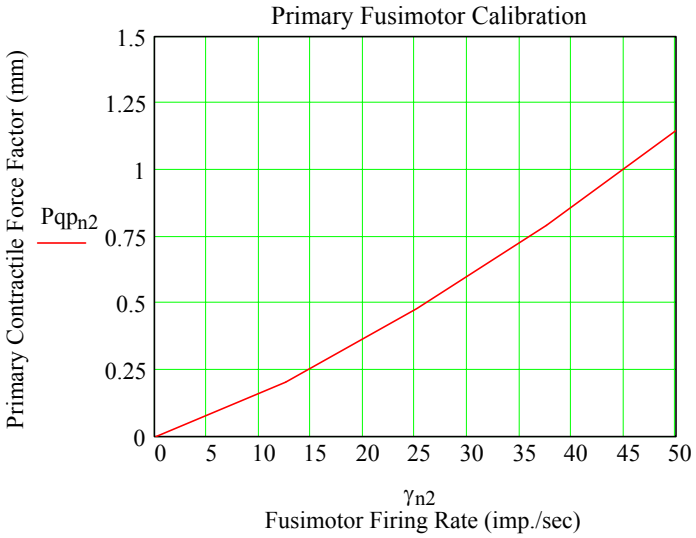

Figure 5: Calibration data for fusimotor excitation of the bag 1 fiber. Pqp is the contractile force factor defined as Q_C/K_{SEC} and has dimensions of mm. γ is the firing rate of the gamma motoneuron. The curve was obtained by forcing the primary afferent firing rate to equal its measured value as a function of fusimotor firing rate at a length of $\lambda = 6.85$ mm. The same calibration curve applies to both the dynamic and the static gamma motoneurons. This curve therefore applies to both bag 1 and bag 2 fibers.

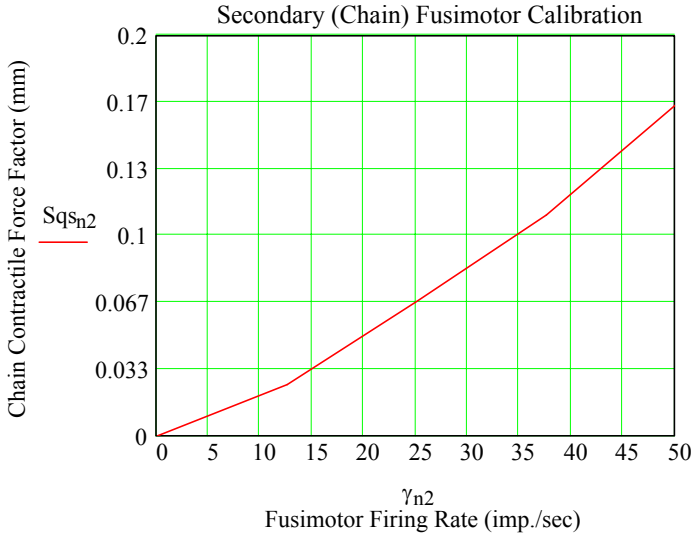

Figure 6: Calibration data for fusimotor excitation of chain fibers. Sqs is the contractile force factor as defined in the caption for figure 5 but applies to chain fibers only.

To obtain any further results we must have a calibration factor relating gamma motoneuron firing rate to the contractile force factor Q_C . This can be done by forcing the model to match measured primary and secondary firing rates for different fusimotor firing rates under isometric (zero velocity) conditions. Figures 5 and 6 provide calibration factors for bag fibers (fig. 5) and for chain fibers (fig. 6). In the solution for the Hill model's ramp response Q_C only appears in the expression as the ratio $q \equiv Q_C / K_{SEC}$ divided by (stiffness ratio plus 1). It is q (in mm) that is plotted in figures 5 and 6. The calibration curves are reasonably linear for fusimotor excitation rates of 12.5 impulses/sec and above. In this region we have

Bag: $q = -0.1 + 0.024 \cdot \gamma$, $\gamma \geq 12.5$ imp/sec = fusimotor firing rate (13a)

Chain: $q = -0.02 + 3.48 \cdot 10^{-3} \gamma$, $\gamma \geq 12.5$ imp/sec (13b).

At lower fusimotor firing rates the calibration curves depart from linear. I have no data available that would allow me to fit the calibration functions in this region, so it seems best to approximate the calibration factors here as

Bag: $q \approx 0.20 \cdot \gamma, \quad \gamma < 12.5$ imp./sec (13c)

Chain: $q \approx 23.5 \cdot 10^{-3} \gamma, \quad \gamma < 12.5$ imp./sec (13d).

The calibration factors presented here were fixed under tonic firing conditions for the gamma motoneurons. Therefore, they reflect only the average (dc) value of Q_C obtained from the dynamical equation for the contractile element.

One shortcoming of this model (linear Hill model plus integrate-and-fire neuron model) is its failure to correctly predict the dynamic indices of either the primary or the secondary afferents under fusimotor stimulation. Our "linear" theory predicts that the dynamic index is insensitive (nearly independent of) Q_C . This is in stark contrast to experimental data, which consistently shows that the dynamic index is a strong function of fusimotor excitation. The model predicts almost no change in dynamic index as a function of fusimotor excitation. The biological mechanism responsible for the observed behavior of dynamic index vs. fusimotor excitation is unknown, but it seems clear that it must be due to some nonlinear effect. It is not known whether this is a failure of the Hill model or something in the dynamics of the sensory neuron or both. The first possibility seems the more likely since measurements show that muscle end plate potentials from fusimotor terminals do not appear to reach the spindle area, and because the linear Hill model ignores the velocity-dependence of the damping factor term *B* due to the Hill equation. On the other hand, the fiber's response to motoneuron excitation involves metabotropic calcium dynamics, and it is not known whether these dynamics penetrate and change the spindle region and/or the afferent nerve endings. At present I have no model, phenomenological or otherwise, that reproduces the dynamic index characteristics as a function of fusimotor excitation.

However, even though the model fails to get at these dynamics, it is still of use to us to examine the peak firing rates, in response to a mechanical ramp, as a function of fusimotor excitation. This is illustrated in Figure 7 for the primary afferent and in Figure 8 for the secondary afferent.

For the primary afferent, figure 7 shows that there is a saturation effect that sets in for velocities above about 25 mm/sec. This would be a problem for the spinal "servo control system" because a saturating feedback measurement of muscle velocity will tend to "open loop" the control system. The application of fusimotor excitation to bag 1 fibers by dynamic gamma motoneurons (in real biological systems) appears to counteract this saturation effect, thereby retaining the information necessary to maintain servo control of the system. Because our model does not correctly produce this effect, our evolved spinal cord neural networks will no doubt depart from their biological counterparts. The discrimination of velocity does not improve very much as fusimotor stimulation increases in our model insofar as the absolute change in firing rate is concerned.

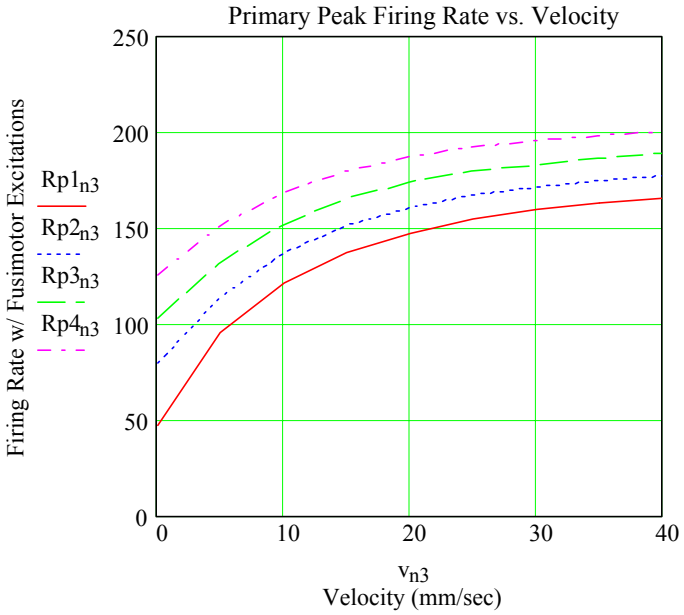

Figure 7: Modeled peak primary afferent firing rate vs. fusimotor excitation and velocity. The responses Rp1 through Rp4 are for q = 0.2, 0.48, 0.79, and 1.15, respectively, applied simultaneously to both the bag 1 and bag 2 fibers.

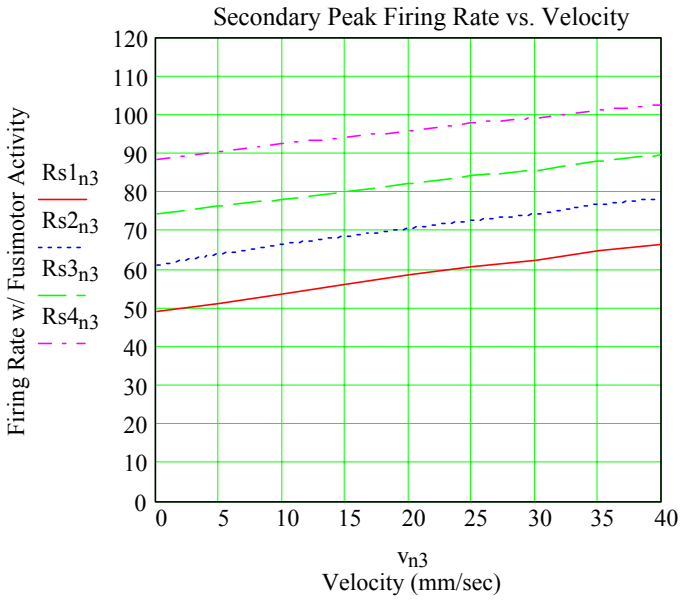

Figure 8: Modeled peak secondary afferent firing rate vs. fusimotor excitation and velocity. The responses Rs1 through Rs4 are for chain fiber q = 0.025, 0.067, 0.110, and 0.165, respectively.

In the case of the secondary afferent response, although the curves shown in figure 8 maintain reasonable linearity as a function of velocity, the absolute change in firing rate is not large for any value of fusimotor stimulation. This is what one would expect from a transducer that is primarily a displacement rather than velocity sensor.

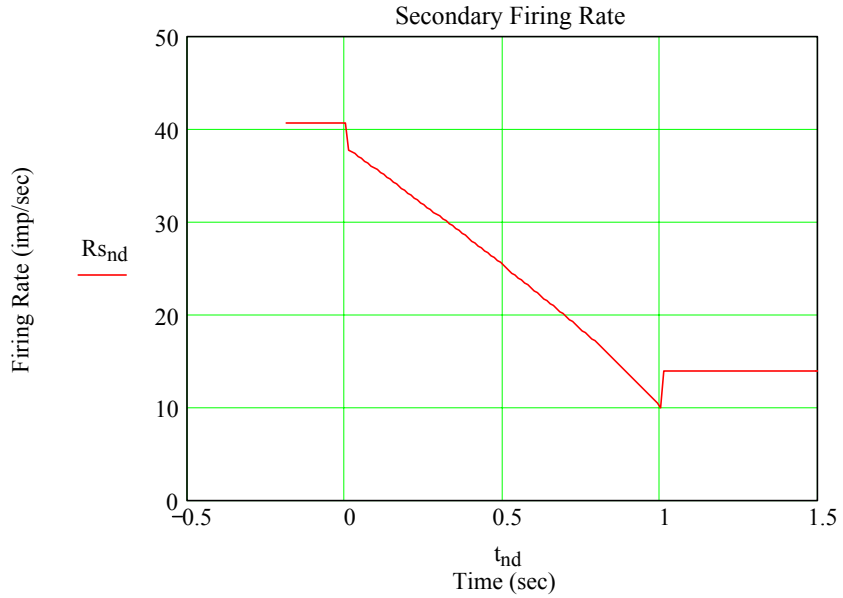

a

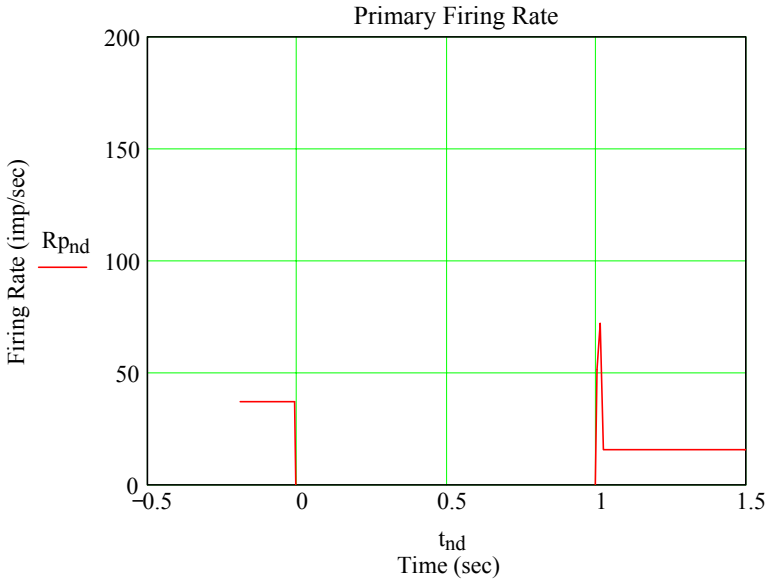

b

Figure 9: Firing rates during ramp contraction. The firing rate of the secondary afferent (a) and the primary afferent (b) are shown for zero fusimotor stimulation and a 5 mm/sec ramped contraction from an initial length of 10 mm to a final length of 5 mm. The secondary maintains its firing rate during contraction. The primary displays the characteristic break in firing and resumes only after the final length is achieved.

IV. Fusimotor Control During Contraction

Although the concern voiced at the end of the previous section is not to be taken lightly, one thing in our favor is that figures 7 and 8 illustrate responses during *stretching* of the muscle.

Because all extrafusal motor control of the system depends on *contraction* due to alpha motoneuron stimulation, *the driving muscle during voluntary movement is always the muscle that is contracting*. Its antagonist muscle (the one being stretched) provides some "fine tuning" of the movement (and assists in posture, which is a low-velocity phenomenon). Fortunately, the discrimination of firing rate during ramp contraction predicted by the model is very good *so long as the spindle afferents continue to fire*. I make the conjecture that it is during contraction that the fusimotor excitation of the spindle plays its most important role. This is what we will discuss in this section.

Figure 9 shows the firing characteristics of the afferents during a 5 mm/sec ramp contraction with no fusimotor firing. Although the secondary afferent firing rate "follows" the muscle length information during the ramp, the primary displays the characteristic "break" in its firing pattern. In effect this "open loops" the spinal control networks that process Ia afferents. This includes the monosynaptic Ia afferent feedback to the alpha motoneurons of the agonist muscle.

Figure 10 illustrates the primary afferent firing rate under fusimotor stimulation. The ramp contraction in this case is the same as in figure 9, but this time the bag 1 fiber is stimulated by firing its dynamic gamma motoneuron. The contractile force factor used in figure 10 is $q = 1.58$, which corresponds to a gamma motoneuron firing rate of 70 imp/sec according to (13a). Although the primary afferent does exhibit some position-dependence in its response, the firing rate is relatively constant during the contraction except for sharp spiking in the rate at the beginning and end of the ramp. Maintenance of closed-loop velocity control is therefore possible in this case.

The firing of secondary afferents can also be interrupted during rapid contraction. Figure 11 illustrates the response of the secondary afferent to a 10 mm/sec ramp contraction with no fusimotor stimulation of the bag 2 or chain fibers. There is a pronounced nonlinearity in response

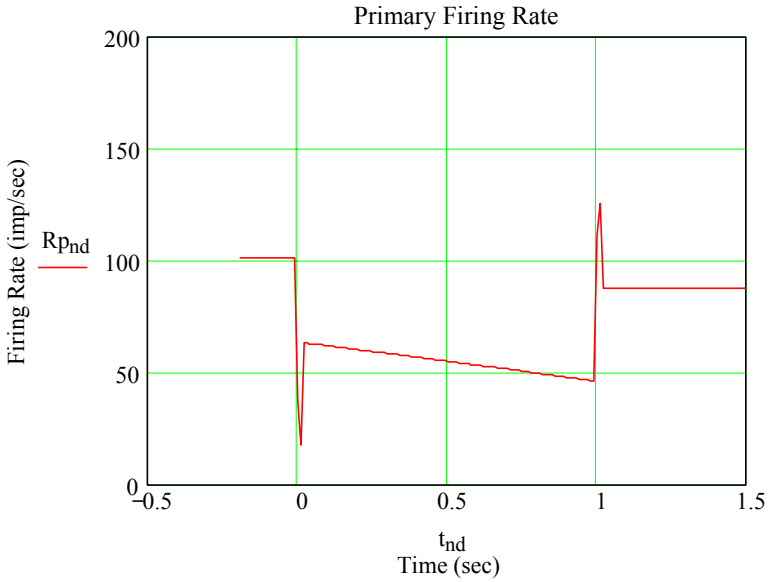

Figure 10: Primary afferent firing rate with dynamic gamma motoneuron stimulation. The ramp conditions are the same as in figure 9 except that the dynamic gamma motoneuron is stimulated at a firing rate of 70 imp/sec ($q = 1.58$). Although the firing rate exhibits some position dependence in its response, the firing rate during the ramp is almost constant except for brief spikes at the beginning and the end.

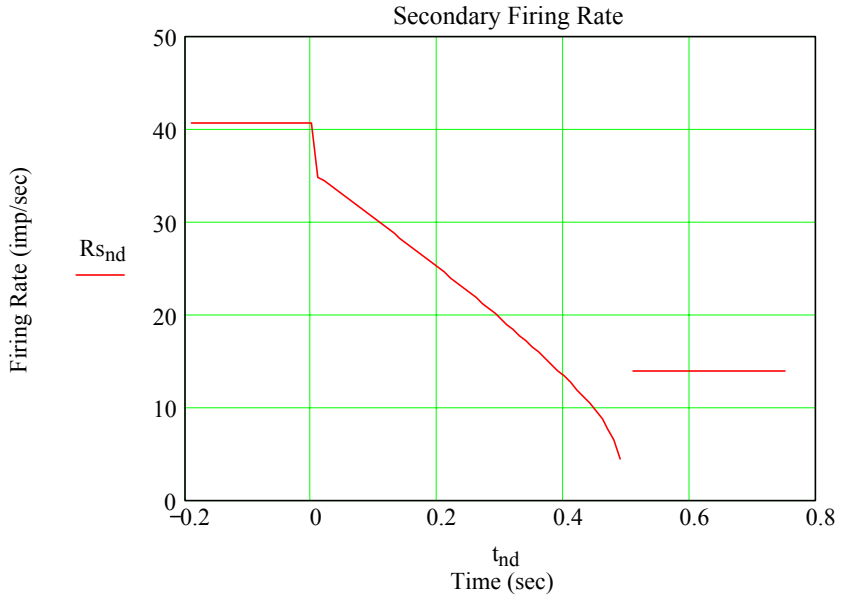

Figure 11: Secondary afferent firing during 10 mm/sec ramp contraction. The graph demonstrates the response under the condition of no fusimotor stimulation of the bag 2 or chain fibers. Note the abrupt drop in firing rate near the end of the ramp followed by a break in firing. This corresponds to the intrafusal fibers in the spindle region becoming so short that the receptor potential drops below the firing threshold of the group II sensory neuron, although the intrafusal fiber does not actually go slack in this case.

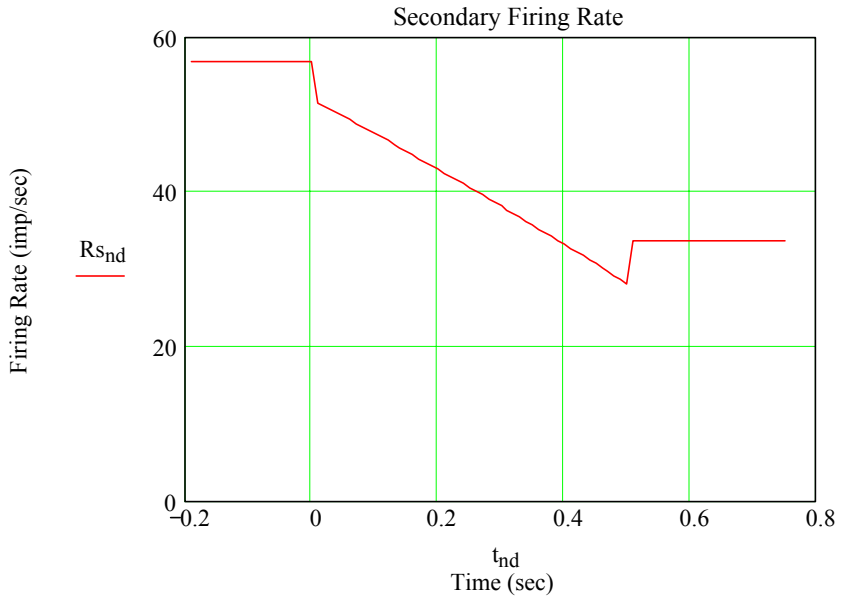

Figure 12: Secondary afferent firing with fusimotor stimulation. The ramp contraction was at 10 mm/sec with chain fiber stimulation by static gamma motoneurons firing at 20 imp/sec.

near the end of the ramp as the intrafusal fiber length in the spindle region shortens to such an extent that the receptor potential drops below the firing threshold of the group II sensory neuron. Figure 12 illustrates the secondary response under the same conditions but with static gamma motoneuron stimulation of the chain fibers at 20 imp/sec (q = 0.05). Fusimotor stimulation restores the linearity of the response and prevents the break in firing observed in figure 11.

We can see from these exhibits that there is a pronounced difference in fusimotor stimulation effects between a ramp extension of the muscle and a ramp contraction. In the former case, the discrimination of position or velocity at high ramp speeds is not improved by fusimotor stimulation. Although the linear model we are working with here does not reproduce the characteristics of the dynamic index properly, the dynamic index is not a measurable quantity to which the spinal neural network has access during a movement. (By definition, the dynamic index compares peak response during the movement with steady-state response after the movement is over). It is likely that sensory discrimination during extension in real (biological) systems is improved by fusimotor stimulation, but it remains the case that the muscle being extended is not the muscle effecting the movement. Therefore the spindle afferents for the extending muscle play at best the role of a dynamic "brake" in helping to control the movement. The main effector of the movement is the contracting muscle that supplies the force required to move the limb, and for this muscle the ability to maintain closed-loop control of the movement is critically affected by fusimotor stimulation.[2]

It is for this reason that I make the conjecture that fusimotor control of the spindle afferents probably evolved mainly due to the performance benefits it has during contraction. If this is true, then it is also possible that whatever effects fusimotor stimulation has during extension could be a mere by-product of the physiology of contraction. This would imply that the extension behavior of fusimotor action might not have been an evolutionary factor so long as this behavior was not actually detrimental to survival. The implication this has for our work is simple: If extension behavior is a secondary consideration, and contraction behavior is the primary consideration, then our approximate model should be sufficient to provide us with afferent feedback signals adequate for the spinal control system's neural networks to accomplish their task.

V. Concluding Remarks

This tech brief has presented a more detailed model of the integrate-and-fire neuron, and it provides the phenomenological constants that reproduce the behavior of biological systems. In our eventual application of this model, and the neural networks coming out of the EC design work based on this model, we will face a scaling requirement. Simply put, biological neurons fire more slowly than our electronic neurons by about 3 orders of magnitude (in the case of the BAN; the difference is even greater for the Frenzel neuron). Yet at the same time, any mechanical platform we eventually build will likely have time constants more or less comparable to those of the biological system. (It takes a great deal more power to move an actuator in milliseconds than to move it in tens or hundreds of milliseconds, and less power implies less weight and a better chance at battery operation of the mechanism). Fortunately, the virtue of an integrator is that its response goes by pulse duty cycle times time, and so it should present no insurmountable problem for our hardware folks to scale firing rate characteristics in our neural networks from the relatively slow ones the EC results will produce to ones that are more compatible with specific electrical and electromechanical characteristics of a robot platform. Frequency scaling is a long-established technique in circuit work, and scaling from biological time constants and firing rates to electromechanical system time constants and firing rates should merely be a matter of our coming up with the proper pulse time modulation scheme.

[2] There is a second order effect of fusimotor stimulation that we should keep in mind. Ia afferents do feed back directly to alpha motoneurons in their respective muscles. Therefore, stimulating Ia afferent firing via fusimotor stimulation of the intrafusal fibers does indirectly excite the alpha motoneurons. It is quite possible that this mechanism may be involved in the recruitment of alpha motoneurons and therefore help to establish the total muscle force being applied to the limb.